

Free-Space Optical Communication Using Non-mode-Selective Photonic Lantern Based Coherent Receiver

Bo Zhang, Renzhi Yuan[†], *Student Member, IEEE*, Jianfeng Sun,
Julian Cheng, *Senior Member, IEEE*, and Mohamed-Slim Alouini, *Fellow, IEEE*

Abstract

A free-space optical communication system using non-mode-selective photonic lantern (PL) based coherent receiver is studied. Based on the simulation of photon distribution, the power distribution at the single-mode fiber end of the PL is quantitatively described as a truncated Gaussian distribution over a simplex. The signal-to-noise ratios (SNRs) for the communication system using PL based receiver are analyzed using different combining techniques, including selection combining (SC), equal-gain combining (EGC), and maximal-ratio combining (MRC). The integral solution, series lower bound solution and asymptotic solution are presented for bit-error rate (BER) of PL based receiver, single-mode fiber receiver and multimode fiber receiver over the Gamma-Gamma atmosphere turbulence channels. We demonstrate that the power distribution of the PL has no effect on the SNR and BER performance of the PL based receiver when MRC is used; and it only has limited influence when EGC is used. However, the power distribution of the PL can greatly affect the BER performance when SC is used. Besides, the SNR gains of the PL based receiver using EGC over single-mode fiber receiver and multimode fiber receiver are numerically studied under different imperfect device parameters; and the scope of application of the communication system is further provided.

Bo Zhang and Jianfeng Sun are with the Key Laboratory of Space Laser Communication and Detection Technology, Shanghai Institute of Optics and Fine Mechanics, Chinese Academy of Sciences, 390 Qinghe Rd., Shanghai 201800, China, (e-mails: zhangbo@siom.ac.cn, sunjianfengs@163.com); Bo Zhang is also with the Center of Materials Science and Optoelectronics Engineering, University of Chinese Academy of Sciences, Beijing 100049, China; Renzhi Yuan and Julian Cheng are with the School of Engineering, The University of British Columbia, Kelowna, V1V 1V7, BC, Canada (e-mails: renzhi.yuan@ubc.ca, julian.cheng@ubc.ca); Mohamed-Slim Alouini is with the Computer, Electrical, and Mathematical Science and Engineering (CEMSE) Division King Abdullah University of Science and Technology (KAUST) Thuwal, Makkah Province, Saudi Arabia (e-mail: slim.alouini@kaust.edu.sa).

[†]: Corresponding author

Index Terms

Equal-gain combining, free-space optical communication, photonic lantern.

I. INTRODUCTION

In satellite communication, coherent free-space optical communication (FSOC) technology is attractive for its high sensitivity and ability to obtain a high data rate [1]–[3]. Recently, researchers have focused on designing coherent optical communication systems using fiber-based transmitters and receivers. Because the fiber-based receiver can make full use of the commercial available components from fiber-optic communication systems, such as fiber transmitter and receiver, erbium-doped fiber amplifiers (EDFAs), and fiber multiplexer and demultiplexer units [4], [5]. However, such implementation has its limitations because the overall efficiency (which will be defined in the sequel) is low.

In a coherent optical communication system using fiber-based receiver, when the signal beam reaches the receiver aperture plane, it is first coupled into the fiber and then mixed with the local oscillator (LO) beam to obtain the mixed signal. There are three important parameters associated with this process: coupling efficiency, mixing efficiency, and overall efficiency. The coupling efficiency is defined as the ratio of the average power coupled into the fiber to the average power in the receiver’s aperture plane [4], [6]–[11]. The mixing efficiency is defined as the ratio of the amplitude of the obtained mixed signal to the amplitude of theoretically mixed signal [12]–[16]. The overall efficiency is defined as the product of the coupling efficiency and the mixing efficiency, which embodies the extent to which the signal beam can be fully utilized. Low overall efficiency can typically degrade signal-to-noise ratio (SNR) [13], [14].

There are two commonly used fiber-based receiver schemes for coherent optical communication systems. The first receiver scheme is the single-mode fiber (SMF) receiver with SMF mixing. The SMF only propagates one field mode. Because the received signal beam and the LO beam propagate in the same SMF, their field modes are the same, i.e., the received signal beam and LO beam fields are matched both spatially and temporally at the detector. Then the mixing efficiency between the LO beam and the signal beam approaches 100% [14]. However, the core diameter of SMF is small ($\sim 10 \mu m$), which limits achievable fiber coupling efficiency, especially in the presence of atmosphere turbulence in free-space channels [4], [6], [7], [12]. For example, the maximum coupling efficiency is 81% in the absence of atmosphere turbulence [6]. For a

TABLE I
COMPARISON BETWEEN SMF RECEIVER AND MMF RECEIVER.

	SMF receiver	MMF receiver
The coupling efficiencies	low	high
The mixing efficiencies	high	low
The overall efficiencies	low	low

moderate strength turbulence ($C_n^2 = 10^{-13} \text{ m}^{-\frac{2}{3}}$, where C_n^2 is refractive-index structure constant), the coupling efficiency is less than 5% [4]. The second receiver scheme is the multimode fiber (MMF) receiver with MMF mixing [8], [9], [13]. The coupling efficiency of MMF, whose core diameter is $\sim 50 \mu\text{m}$ [9], is much higher than that of the SMF [10], [13], [17]–[19]. However, only the portion of the signal beam that is in the same temporal and spatial mode of the LO beam can produce high mixing efficiency [13]. The MMF contains not only the fundamental mode component, but also high-order mode components. Then the mixing efficiency between the LO beam and the signal beam will be degraded [13], [19], [20]. For example, the coupling efficiency of MMFs tested in [9] is greater than 95%; for asymmetric square waveguide supporting seventy-five distinct modes tested in [13], the coupling efficiency for MMF receiver is 75-78%; the mixing efficiency is 21-23%, and the overall efficiency becomes only 11-17%. The properties of the SMF receiver and MMF receiver are summarized in Table I. From Table I, we can conclude that both SMF receiver and MMF receiver have low overall efficiency.

Recently, a non-mode-selective photonic lantern (PL) based coherent optical receiver has been proposed, and the overall efficiency of this receiver can be improved [20]–[24]. Fig. 1 shows the schematic diagram of a PL [25], [26]. In this diagram, one end of the PL is a relatively-large multimode core, and the other end is an array of several relatively-small single-mode cores. In between is a transition region ¹. Fig. 2 shows a structural diagram of a complete coherent FSOC system based on non-mode-selective PL. The signal beam is transmitted from the transmitter, and is coupled into the receiver after passing through the atmosphere turbulence. In the receiver, the large-core MMF end of the PL is placed behind the receiver len to collect the multimode signal

¹There are two types of PLs [26], [27]: mode-selective PL [28], [29] and non-mode-selective PL [20]–[23]. In a mode-selective PL, the single-mode cores are designed for transmitting light with different electromagnetic wave modes. While in a non-mode-selective PL, the single-mode cores are designed for transmitting light having the same electromagnetic wave mode. This paper focuses on the non-mode-selective PL.

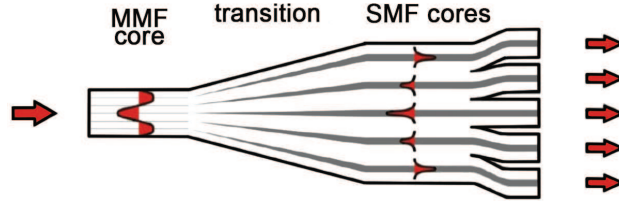


Fig. 1. Structural diagram of a PL [25]

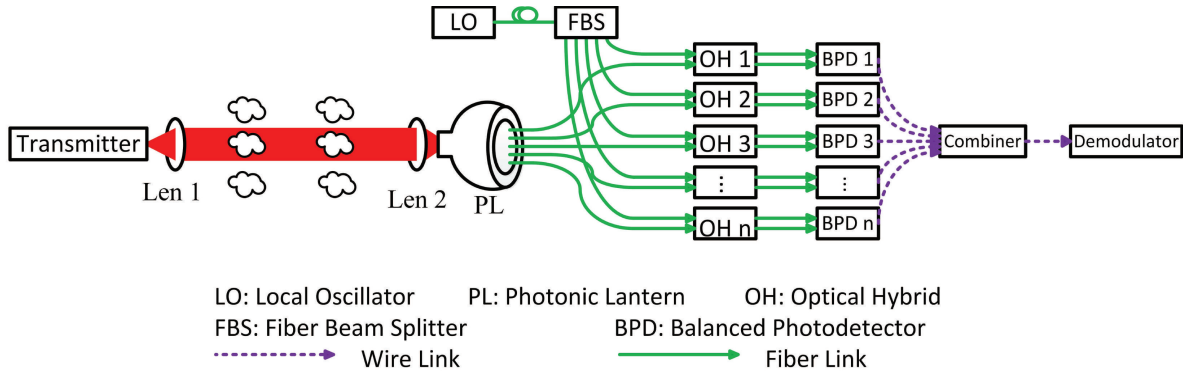


Fig. 2. Structural diagram of a coherent FSOC system based on non-mode-selective PL

beam. Then the PL converts the multimode signal beam into N single-mode signal beams. The single-mode LO beam is split into N equal parts by a fiber beam splitter (FBS). Each single-mode signal beam of the PL is mixed with a single-mode LO beam in an optical hybrid. After that, each mixed signal is converted into an electrical signal by the corresponding balanced photodetector. All the electrical signals are sent to the combiner and the demodulator for processing. The system can fully take advantage of the MMF, which has higher coupling efficiency compared with the SMF, and can take advantage of the SMF that has nearly 100% mixing efficiency with the single-mode LO beam [21].

A recent work [30] investigated the performance of coherent FSOC receiver under moderate-to-strong turbulence. However, the effect of the power distribution at SMF end of the PL on SNR was not studied. From [26], we know that the power distribution at SMF end of non-mode-selective PL varies according to input mode profiles, input pointing errors, and temperature or pressure variations on the MMF section of the PL. In FSOC, the signal beam impaired by atmospheric turbulence contains not only the fundamental mode component but also the higher-

order mode components, and the influence of atmospheric turbulence on signal beam changes with time and space. Then the mode profile of the signal beam coupled into MMF end of the PL will change with time, resulting in the power distribution variation at SMF end of a non-mode-selective PL. As a result, the SNR of the coherent optical receiver based on PL will change [24]. Therefore, it is necessary to study the power distribution at SMF end of the PL. In [24], we proposed two different distributions: the multivariate Gaussian distribution over a simplex for small power fluctuation case and the uniform distribution over a simplex for large power fluctuation case, to describe the power distribution at SMF end of non-mode selective PL. It was found that different power distributions can have different effects on SNR, and when the number of single-mode fibers of the PL is equal to the number of guided modes at multimode end of the PL, the average SNR attains its maximum value [24].

Different from [24], this paper proposes a more accurate power distribution: truncated Gaussian distribution over a simplex, and this proposal is based on the simulation results of photon distribution in Section II-B. In addition, the SNRs of the communication system using PL based receiver are analyzed using different combining techniques, including selection combining (SC), equal-gain combining (EGC), and maximal-ratio combining (MRC); and they are compared with traditional SMF and MMF receivers in Section III. The bit-error rate (BER) performance of a binary phase-shift keying (BPSK) system is analyzed. The integral solution, lower bound series solution and asymptotic solution of the BER are presented. The BER performance of the system using different combining techniques are studied and compared with the traditional SMF and MMF receivers over the Gamma-Gamma atmosphere turbulence channels in Section IV. We demonstrate that the power distribution of the PL has no effect on the SNR and BER performance of the PL based receiver when MRC is used. Simulation results in Section V show that the power distribution of the PL has only limited influence on the BER performance of PL based receiver when EGC is used; and the power distribution can greatly affect the BER performance when SC is used. Besides, the SNR gains of the PL based receiver using EGC over the SMF receiver and MMF receivers are numerically calculated under different imperfect device parameters; and the scope of application of the communication system is further provided. To the best of the authors' knowledge, this is the first analytical study on the influences of the power distribution of the PL on the performance of different combining techniques. Our findings can provide some useful guidelines for the design of PL based receiver for FSOC systems.

II. SYSTEM MODEL

A. Free-Space Atmosphere Channel

In FSO, atmospheric turbulence introduces fluctuation of irradiance, which results in fluctuation of SNR. The probability density function (PDF) of the received signal irradiance can be modeled as a Gamma-Gamma distribution [31], [32], which emerges as a useful turbulence model as it has excellent fit with measurement data over a wide range of turbulence conditions [31]. The PDF of the received signal irradiance I ($I > 0$) is given by

$$f(I) = \frac{2(\alpha\beta)^{\frac{\alpha+\beta}{2}}}{\Gamma(\alpha)\Gamma(\beta)} I^{\frac{\alpha+\beta}{2}-1} K_{\alpha-\beta}(2\sqrt{\alpha\beta I}), \quad (1)$$

where $\Gamma(\cdot)$ is the Gamma function; $K_{\alpha-\beta}(\cdot)$ is the modified Bessel function of the second kind with order $\alpha - \beta$. The parameters α and β are directly related to the atmospheric conditions [31], and they respectively denote the effective numbers of large-scale and small-scale cells of the scattering process, respectively. Without loss of generality, the received signal irradiance I is normalized, i.e., $E[I] = 1$, where $E[\cdot]$ denotes the mathematical expectation.

B. Power Distribution in PL

When the signal beam transmitted from the transmitter reaches the receiver system after passing through the atmosphere turbulence, it is coupled into the MMF end of the PL. We assume the power received at MMF end of the PL is P_M , then we have [33]

$$P_M = \zeta_M AI, \quad (2)$$

where ζ_M is the coupling efficiency of MMF, and A is the area of receiving aperture of the lens. When the PL converts the multimode signal beam into N single-mode signal beams, loss will be introduced [26]. If we denote the loss factor of the PL by ξ_{PL} ($0 < \xi_{PL} \leq 1$), then the output optical power of the PL is $P_S = \xi_{PL} P_M$.

For a PL with N SMFs, if we denote the power distributed at each SMF end by $P_{S,i}$ ($i = 1, 2, \dots, N$) and denote the ratio of $P_{S,i}$ to P_S by a_i , then we have

$$P_{S,i} = a_i P_S = a_i \xi_{PL} \zeta_M AI, \quad (3)$$

where random variables (RVs) a_i ($i = 1, 2, \dots, N$) satisfy

$$a_1 + a_2 + \dots + a_N = 1, \quad 0 \leq a_i \leq 1, \quad i = 1, 2, \dots, N, \quad (4)$$

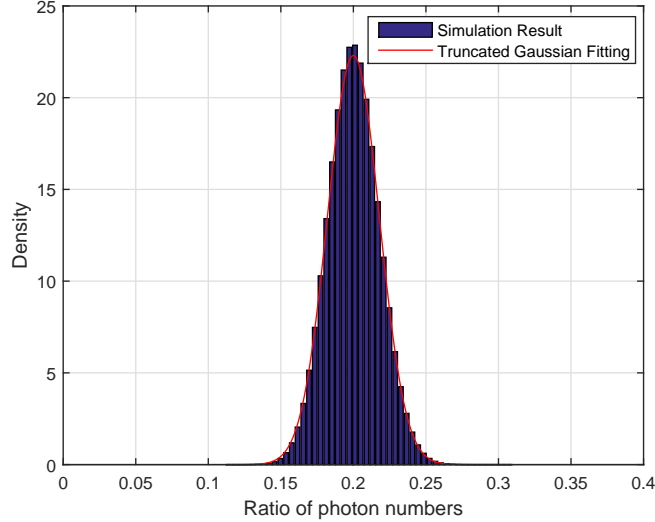


Fig. 3. The obtained ratio distribution for one SMF end of the PL with $N = 5$, $M = 500$, and $L = 10^7$ (The range of a_i is between 0 and 1. For simplicity, we only plot the range of a_i from 0 to 0.4.)

where the set of $\{a_1, a_2, \dots, a_N\}$ that satisfies (4) is called a standard unit simplex [34].

The exact power distribution at SMF end of the PL is not known. Because the optical power is proportional to the photon number, the ratios $\{a_1, a_2, \dots, a_N\}$ for the optical power is identical to the ratios for the photon numbers. Therefore, we can simulate the photon distribution to obtain the power distribution.

1) *Simulation Model For Photon Distribution:* Here, we use a Monte-Carlo method to simulate the photon distribution at SMF end of the PL. We denote the number of SMF of the PL by N . Because the loss of PL has no effect on the power distribution at SMF end of the PL, we do not consider the loss of PL in the simulation of photon distribution. Because this work assumes non-mode-selective PL, it is reasonable to assume that each SMF of a PL is exactly the same. Then the probability of each photon at MMF end assigned to any SMF of PL is assumed the same. Therefore, the explicit Monte-Carlo process can be summarized as follows: Step 1, we first generate M photons and assign each photon into one SMF end randomly; Step 2, we calculate and record the ratio of the photon number m_i of i th SMF end to the total photon number M as $a_i = m_i/M$, where $i = 1, 2, \dots, N$; Step 3, repeat Step 1 and Step 2 L times. Then we can obtain the distribution of a_i from its L samples for the i th SMF and obtain the correlation coefficient between a_i and a_j for $i \neq j$.

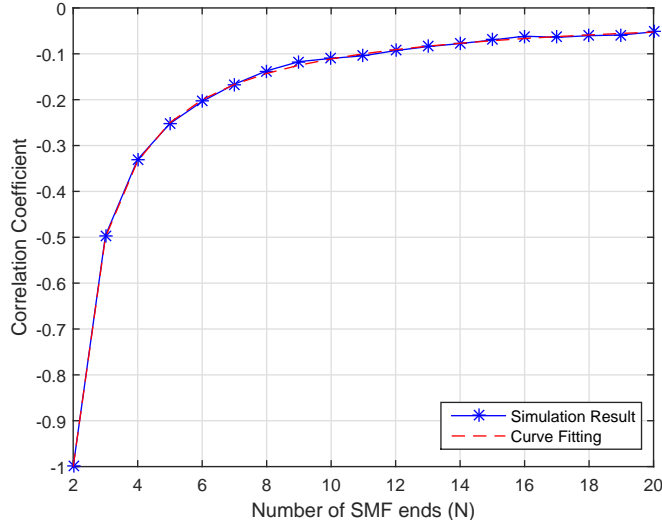


Fig. 4. The obtained correlation coefficient between the ratios of two distinct SMF with $M = 100 \times N$ and $L = 10^7$

The obtained distribution of the ratio a_i for some SMF end is shown in Fig. 3. We find that the photon number distribution at the i th SMF end of the PL has excellent fit with the truncated Gaussian distribution with mean value $1/N^2$. The obtained correlation coefficients between the ratios of two distinct SMF over the number of SMF ends are shown in Fig. 4. We can see that the correlation coefficients between the ratios of two distinct SMFs are always negative, which is due to the constraint (4). Besides, we can see that the correlation coefficient between two SMFs increases as N increases. For example, when $N = 2$, according to the constraint (4), the correlation coefficient between two SMFs is -1 . As N approaches ∞ , the correlation coefficient between two SMFs should approach 0. We also perform the curve fitting on the simulation results and find that the correlation coefficients can be fitted as $-\frac{1}{N-1}$, which coincides to the analytical result obtained in Section II-B2.

2) *Truncated Multivariate Gaussian Model For Power Distribution:* According to above simulation results, it is reasonable to assume that the ratios $\mathbf{a} = [a_1, a_2, \dots, a_N]^T$ for the optical power satisfies a truncated multivariate Gaussian distribution [35] over the simplex defined in (4). The mathematical expectation of this truncated multivariate Gaussian distribution

²We remark that the obtained variance of a_i can vary as the number of simulation repeating times varies due to the converging property of the Monte-Carlo method. A large number of repeating times results in a small variance. However the correlation coefficient between a_i and a_j is independent of the number of repeating times

is $E[\mathbf{a}] = \boldsymbol{\mu}_a = [\frac{1}{N}, \frac{1}{N}, \dots, \frac{1}{N}]^T$, where $[\cdot]^T$ represents the transpose operator³. Here we derive the PDF of this truncated multivariate Gaussian distribution analytically.

We first remove the constraint $a_1 + a_2 + \dots + a_N = 1$, then the joint PDF of the truncated multivariate Gaussian distribution has the following form:

$$f(\mathbf{a}) = \frac{1}{C_1} \exp \left\{ -\frac{1}{2} [\mathbf{a} - \boldsymbol{\mu}_a]^T \boldsymbol{\Sigma}_a^{-1} [\mathbf{a} - \boldsymbol{\mu}_a] \right\}, \quad (5)$$

$$0 \leq a_i \leq 1, \quad i = 1, 2, \dots, N,$$

where $C_1 = \int_V \exp \left\{ -\frac{1}{2} [\mathbf{a} - \boldsymbol{\mu}_a]^T \boldsymbol{\Sigma}_a^{-1} [\mathbf{a} - \boldsymbol{\mu}_a] \right\} dV$ is a constant number for normalization; V is the domain defined as $V = \{0 \leq a_i \leq 1, i = 1, 2, \dots, N\}$; $\boldsymbol{\Sigma}_a$ is the covariance matrix of \mathbf{a} . Because this work assumes non-mode-selective PL, it is reasonable to assume that a_1, a_2, \dots, a_N have the same Gaussian variance⁴ $var(a_i) = \sigma^2, i = 1, 2, \dots, N$; and the Gaussian covariances $cov(a_i, a_j)$ for any a_i and a_j , when $i \neq j, i, j = 1, 2, \dots, N$, are the same. Then the $N \times N$ dimensional Gaussian covariance matrix $\boldsymbol{\Sigma}_a$ can be written as

$$\boldsymbol{\Sigma}_a = \sigma^2 \begin{bmatrix} 1 & \rho & \cdots & \rho \\ \rho & 1 & \cdots & \rho \\ \vdots & \vdots & \ddots & \vdots \\ \rho & \rho & \cdots & 1 \end{bmatrix}, \quad (6)$$

where $\rho = \frac{cov(a_i, a_j)}{\sigma^2}$ is the correlation coefficient between a_i and a_j when $i \neq j, i, j = 1, 2, \dots, N$. Then inverse matrix $\boldsymbol{\Sigma}_a^{-1}$ in (5) can be obtained as

$$\boldsymbol{\Sigma}_a^{-1} = \frac{1}{[1 + (N-1)\rho](1-\rho)\sigma^2} \times \begin{bmatrix} 1 + (N-2)\rho & -\rho & \cdots & -\rho \\ -\rho & 1 + (N-2)\rho & \cdots & -\rho \\ \vdots & \vdots & \ddots & \vdots \\ -\rho & -\rho & \cdots & 1 + (N-2)\rho \end{bmatrix}. \quad (7)$$

However, when the constraint $a_1 + a_2 + \dots + a_N = 1$ is considered, the covariance matrix $\boldsymbol{\Sigma}_a$ becomes a rank-deficient matrix and it has no inverse matrix. We first derive the correlation

³Our analysis can be easily extended to the cases where different SMF ends have different mean values by replacing $\boldsymbol{\mu}_a$ with the actual mean values.

⁴Note that the Gaussian variance $var(a_i)$ here is not the actual variance of a_i . This is because the multivariate Gaussian distribution characterized is truncated by the definition domain V . Then the actual variance $var_{Actual}(a_i)$ is defined as $var_{Actual}(a_i) \triangleq \int_V (a_i - 1/N)^2 f(\mathbf{a}) dV$, which is smaller than the Gaussian variance $var(a_i)$.

coefficient ρ . The constraint $a_1 + a_2 + \dots + a_N = 1$ can be rewritten as $[\mathbf{a} - \boldsymbol{\mu}_a]^\top \mathbf{1} = 0$, where $\mathbf{1} = [1, 1, \dots, 1]^\top$ is an $N \times 1$ dimensional vector. Then we have [24]

$$\begin{aligned} E [[\mathbf{a} - \boldsymbol{\mu}_a][\mathbf{a} - \boldsymbol{\mu}_a]^\top \mathbf{1}] &= \boldsymbol{\Sigma}_a \mathbf{1} \\ &= \sigma^2(1 + (N - 1)\rho)\mathbf{1} \\ &= \mathbf{0}, \end{aligned} \quad (8)$$

where $\mathbf{0} = [0, 0, \dots, 0]^\top$ is an $N \times 1$ dimensional zero vector. Therefore, the correlation coefficient ρ can be obtained from (8) as $\rho = -\frac{1}{N-1}$, which is the same as the correlation coefficient obtained from the simulation result in Fig. 4. This correlation coefficient is also consistent with the inverse matrix in (7) because the numerator of $\boldsymbol{\Sigma}_a^{-1}$ becomes zero when $\rho = -\frac{1}{N-1}$, and thus the inverse matrix does not exist.

To obtain the explicit form of the joint PDF, we generalize a generalized inverse matrix of $\boldsymbol{\Sigma}_a$, and let $\rho \rightarrow -\frac{1}{N-1}$ when the constraint $a_1 + a_2 + \dots + a_N = 1$ is considered. Then the joint PDF of \mathbf{a} can be obtained by substituting (7) into (5) and letting $\rho \rightarrow -\frac{1}{N-1}$. After some algebra (see Appendix A), the joint PDF can be obtained as

$$\begin{aligned} f(\mathbf{a}) &= \frac{1}{C_2} \exp \left\{ -\frac{1}{2} [\mathbf{a}^* - \boldsymbol{\mu}_{a^*}]^\top \boldsymbol{\Sigma}_{a^*}^{-1} [\mathbf{a}^* - \boldsymbol{\mu}_{a^*}] \right\} \\ &\quad \times \delta(a_1 + a_2 + \dots + a_N - 1), \\ &\quad 0 \leq a_i \leq 1, \quad i = 1, 2, \dots, N, \end{aligned} \quad (9)$$

where

$$\begin{aligned} C_2 &= \int_V \exp \left\{ -\frac{1}{2} [\mathbf{a}^* - \boldsymbol{\mu}_{a^*}]^\top \boldsymbol{\Sigma}_{a^*}^{-1} [\mathbf{a}^* - \boldsymbol{\mu}_{a^*}] \right\} \\ &\quad \times \delta(a_1 + a_2 + \dots + a_N - 1) dV \end{aligned} \quad (10)$$

is a constant normalization factor; $\mathbf{a}^* = [a_1, a_2, \dots, a_{N-1}]^\top$ is an $(N-1) \times 1$ dimensional vector; $\boldsymbol{\mu}_{a^*} = [\frac{1}{N}, \frac{1}{N}, \dots, \frac{1}{N}]^\top$ is an $(N-1) \times 1$ dimensional vector; and the covariance matrix $\boldsymbol{\Sigma}_{a^*}$ for \mathbf{a}^* is the first $(N-1) \times (N-1)$ dimensional submatrix of $\boldsymbol{\Sigma}_a$. Then the inverse of $\boldsymbol{\Sigma}_{a^*}$ can be obtained as

$$\boldsymbol{\Sigma}_{a^*}^{-1} = \frac{N-1}{N\sigma^2} \begin{bmatrix} 2 & 1 & \dots & 1 \\ 1 & 2 & \dots & 1 \\ \vdots & \vdots & \ddots & \vdots \\ 1 & 1 & \dots & 2 \end{bmatrix}. \quad (11)$$

C. Two Extreme Cases

Here we present two extreme cases of the truncated Gaussian distribution: the (joint) degenerate distribution and the (joint) uniform distribution, corresponding to the cases of minimum Gaussian variance $\sigma^2 = 0$ and maximum Gaussian variance ⁵ $\sigma^2 = \infty$, respectively.

1) *Degenerate Distribution Case:* For a degenerate distribution, $a_i = \frac{1}{N}, i = 1, 2, \dots, N$ with probability one. Therefore, the joint PDF can be expressed as

$$f(\mathbf{a}) = \prod_{i=1}^N \delta(a_i - \frac{1}{N}). \quad (12)$$

2) *Uniform Distribution Case:* For an uniform distribution, $a_i, i = 1, 2, \dots, N$ is uniformly distributed on $[0, 1]$. The explicit joint PDF can be obtained by letting $\sigma^2 \rightarrow \infty$ in (9), i.e.,

$$f(\mathbf{a}) = \lim_{\sigma^2 \rightarrow \infty} \frac{\exp\{-\frac{1}{2}[\mathbf{a}^* - \boldsymbol{\mu}_{\mathbf{a}^*}]^T \boldsymbol{\Sigma}_{\mathbf{a}^*}^{-1} [\mathbf{a}^* - \boldsymbol{\mu}_{\mathbf{a}^*}]\} \delta(a_1 + a_2 + \dots + a_N - 1)}{C_2}. \quad (13)$$

From the expression of $\boldsymbol{\Sigma}_{\mathbf{a}^*}^{-1}$ in (11), we can find that the exponential term in (13) approaches one when $\sigma^2 \rightarrow \infty$. Similarly, for the denominator C_2 , we have

$$\begin{aligned} \lim_{\sigma^2 \rightarrow \infty} C_2 &= \int_V \delta(a_1 + a_2 + \dots + a_N - 1) dV \\ &= \int_{V_s} dV_s \\ &= \frac{1}{(N-1)!}, \end{aligned} \quad (14)$$

where $V_s = \frac{1}{(N-1)!}$ is the volume of the standard simplex defined in (4). Substituting (14) into (13), we can obtain the joint PDF as

$$f(\mathbf{a}) = (N-1)! \delta(a_1 + a_2 + \dots + a_N - 1). \quad (15)$$

III. SIGNAL-TO-NOISE RATIO

We assume that the shot noise is the dominated noise source in the coherent receiver, which is reasonable due to the presence of high intensity LO beams in balanced photodetectors. When the output signals of the SMF ends are combined using EGC ⁶, the instantaneous SNR can be obtained as [24]

$$\gamma_{PL}^{EGC} = \frac{R\eta_S \left(\sum_{i=1}^N \sqrt{P_{S,i}} \right)^2}{NqB}, \quad (16)$$

⁵The actual variance of a_i is $\frac{1}{12}$, because a_i is uniformly distributed on $[0, 1]$.

⁶Here EGC method is used to combine the output signals of all SMF ends of the PL. Because there is only one receiving port and no diversity technique is introduced, the name ‘‘EGC’’ should not be confused with the diversity combining technique EGC in wireless communications.

where R is the responsivity of the photodiode; η_S is the mixing efficiency of SMF; q is the electronic charge and B is the noise equivalent bandwidth of the detector. Substituting $P_{S,i}$ into γ_{PL} , we can obtain

$$\gamma_{PL}^{EGC} = K \left(\sum_{i=1}^N \sqrt{a_i} \right)^2 I, \quad (17)$$

where $K = \frac{RA\zeta_M \xi_{PL} \eta_S}{NqB}$.

Then the average SNR of coherent FSOC system using PL based receiver with EGC is

$$\begin{aligned} \bar{\gamma}_{PL}^{EGC} &= E[\gamma_{PL}] \\ &= KE \left[\left(\sum_{i=1}^N \sqrt{a_i} \right)^2 \right] E[I] \\ &= K [1 + N(N-1)E[\sqrt{a_1 a_2}]], \end{aligned} \quad (18)$$

where we have used the assumption $E[I] = 1$ and the equality $E \left[\left(\sum_{i=1}^N \sqrt{a_i} \right)^2 \right] = 1 + N(N-1)E[\sqrt{a_1 a_2}]$.

Similarly, the instantaneous and average SNR for SC can be respectively obtained as

$$\gamma_{PL}^{SC} = KN \max_i \{a_i\} I \quad (19)$$

and

$$\bar{\gamma}_{PL}^{SC} = KNE \left[\max_i \{a_i\} \right]. \quad (20)$$

The instantaneous and average SNR for MRC can be respectively obtained as

$$\begin{aligned} \gamma_{PL}^{MRC} &= KN \sum_{i=1}^N a_i I \\ &= KNI \end{aligned} \quad (21)$$

and

$$\bar{\gamma}_{PL}^{MRC} = KN. \quad (22)$$

An important observation is that the instantaneous and average SNR for MRC are irrelevant to the power distribution of the PL due to the relation $\sum_{i=1}^N a_i = 1$. Since the BER is determined by the instantaneous SNR, we can also conclude that the power distribution of the PL has no effect on the BER performance of the PL based receiver when MRC is used. This is a unique feature of the MRC for PL based receiver. However, the MRC requires the measurements of both the amplitude and the phase of the signal in each branch, which is more complex compared

with other combining techniques. In practical implementation, EGC and SC are two widely used combining techniques.

For the average SNR of EGC or SC, it is challenging to obtain an analytical expression for $E[\sqrt{a_1 a_2}]$ in (18) or $E[\max_i\{a_i\}]$ in (20) when a general truncated multivariate Gaussian distribution is considered. However, it is still meaningful to consider the extreme cases defined in II-C, because the degenerate case and the uniform case correspond to the smallest and the largest variance of the signal strength in each branch, respectively.

A. Degenerate Distribution Case

For the degenerate distribution, $a_i = \frac{1}{N}$, ($i = 1, 2, \dots, N$) and we have $E\left[\left(\sum_{i=1}^N \sqrt{a_i}\right)^2\right] = N$ and $E[\max_i\{a_i\}] = \frac{1}{N}$. Then the average SNR for EGC and SC become

$$\bar{\gamma}_{PL, Deg}^{EGC} = KN \quad (23)$$

and

$$\bar{\gamma}_{PL, Deg}^{SC} = K. \quad (24)$$

The average SNR of the EGC in degenerate distribution case equals the average SNR of the MRC. This is because all the branches have the same signal strength, then the EGC becomes an MRC.

B. Uniform Distribution Case

For the uniform distribution, a_i , ($i = 1, 2, \dots, N$) is uniform distributed in $[0, 1]$ and we can obtain $E[\sqrt{a_1 a_2}] = \frac{\pi}{4N}$ (see Appendix B). Then the average SNR for EGC becomes

$$\bar{\gamma}_{PL, Uni}^{EGC} = K \frac{\pi N + 4 - \pi}{4}. \quad (25)$$

However, it is still challenging to obtain an analytical form of average SNR of SC for uniform distribution case, except for the case with $N = 2$. When $N = 2$, we have $E[\max_i\{a_i\}] = \frac{3}{4}$. When $N > 2$, we can use the Monte-Carlo method to numerically obtain $E[\max_i\{a_i\}]$ and then use the curve fitting method to approximate $E[\max_i\{a_i\}]$ as $\frac{4.45}{N+4.33}$. Then the average SNR for SC can be obtained as

$$\bar{\gamma}_{PL, Uni}^{SC} \approx K \frac{4.45N}{N + 4.33}. \quad (26)$$

C. General Distribution Case

For a general truncated multivariate Gaussian distribution, i.e., $0 < \sigma^2 < \infty$, the average SNR is between the SNR of degenerate distribution and the SNR of uniform distribution. Now we consider the average SNR ratio of the degenerate distribution over the uniform distribution.

For the EGC, we have

$$\frac{\bar{\gamma}_{PL, Deg}^{EGC}}{\bar{\gamma}_{PL, Uni}^{EGC}} = \frac{4N}{\pi N + 4 - \pi}, \quad (27)$$

which is between $\frac{8}{4+\pi} \approx 1.12$ when $N = 2$ and $\frac{4}{\pi} \approx 1.27$ when $N = \infty$. This implies that the influence of the power distribution of PL on the average SNR is relatively small when EGC method is used for signal combining.

For the SC, we have

$$\frac{\bar{\gamma}_{PL, Deg}^{SC}}{\bar{\gamma}_{PL, Uni}^{SC}} \approx \frac{N + 4.33}{4.45N}, \quad (28)$$

which is between 0.667 when $N = 2$ and 0.225 when $N = \infty$. Since $\frac{\bar{\gamma}_{PL, Deg}^{SC}}{\bar{\gamma}_{PL, Uni}^{SC}}$ is always smaller than one, an interesting observation is that the SC prefers a large variance σ^2 than a small one. This is because the SC selects the largest a_i as the output, then a larger variance of a_i can have a larger possibility of obtaining a large a_i .

D. Signal-to-Noise Ratios for SMF and MMF receivers

For comparison, we also present the SNR of the SMF receiver and MMF receiver here. When shot noise is the dominated noise, the instantaneous SNR of the SMF receiver is

$$\gamma_{SMF} = \frac{\zeta_S \eta_S R A}{qB} I, \quad (29)$$

where ζ_S is the coupling efficiency of SMF; and the average SNR of SMF is

$$\bar{\gamma}_{SMF} = E[\gamma_{SMF}] = \frac{\zeta_S \eta_S R A}{qB}. \quad (30)$$

Similarly, the instantaneous SNR of the MMF receiver is

$$\gamma_{MMF} = \frac{\zeta_M \eta_M R A}{qB} I, \quad (31)$$

where η_M is the mixing efficiency of MMF mixer; and the average SNR of MMF is

$$\bar{\gamma}_{MMF} = E[\gamma_{MMF}] = \frac{\zeta_M \eta_M R A}{qB}. \quad (32)$$

IV. BIT-ERROR RATE

A. Integral Expression of BER

The BER conditioned on received signal irradiance I and power distribution \mathbf{a} for an FSOC BPSK system ⁷ using PL based receiver is given by [36]

$$P_{e,PL}(I, \mathbf{a}) = Q(\sqrt{\gamma_{PL}}), \quad (33)$$

where $Q(\cdot)$ is the Gaussian Q -function; and γ_{PL} is the instantaneous SNR, which can be obtained in (17), (19), and (21) for EGC, SC, and MRC, respectively. Then the unconditional BER for PL based receiver can be obtained as the following integral form

$$P_{e,PL} = \int_0^\infty \int_V f(I) f(\mathbf{a}) Q(\sqrt{\gamma_{PL}}) d\mathbf{a} dI, \quad (34)$$

where $f(I)$ is the PDF of the signal irradiance I given in (1), and $f(\mathbf{a})$ is the joint PDF of power ratios \mathbf{a} given in (9).

Similarly, the unconditional BERs for SMF receiver and MMF receiver are obtained as

$$P_{e,SMF} = \int_0^\infty f(I) Q(\sqrt{\gamma_{SMF}}) dI \quad (35)$$

and

$$P_{e,MMF} = \int_0^\infty f(I) Q(\sqrt{\gamma_{MMF}}) dI, \quad (36)$$

respectively.

B. Analytical Lower Bound For BER

Because $\left(\sum_{i=1}^N \sqrt{\hat{a}_i}\right)^2 \leq N$, where the equal sign is obtained when $a_i = \frac{1}{N}, i = 1, 2, \dots, N$, we have $\gamma_{PL}^{EGC} \leq KNI = \gamma_{PL}^{MRC}$. Besides, noting that $\max_i \{a_i\} \leq 1$, we have $\gamma_{PL}^{SC} \leq KNI = \gamma_{PL}^{MRC}$. Therefore, the SNR of PL based receiver is bounded by the SNR of MRC ⁸. Then we can obtain a lower bound for $P_{e,PL}$ as

$$\begin{aligned} P_{e,PL}^{lower} &= \int_0^\infty \int_V f(I) f(\mathbf{a}) Q\left(\sqrt{KNI}\right) d\mathbf{a} dI \\ &= \int_0^\infty f(I) Q\left(\sqrt{\bar{\gamma}_{PL}^{MRC} I}\right) dI, \end{aligned} \quad (37)$$

⁷Although we only present the BER for BPSK scheme here, the BER and symbol error rate (SER) for other coherent modulation schemes can be easily found in a similar way.

⁸This coincides with the fact that MRC is the optimal combining regarding the SNR performance.

which is also the unconditional BER of PL based receiver using MRC.

Then we can obtain an analytical expression of the lower bound (37) by using a series expansion of the modified Bessel function of the second kind in (1) as [36]

$$K_v(x) = \frac{\pi}{2 \sin(\pi v)} \sum_{p=0}^{\infty} \left[\frac{(x/2)^{2p-v}}{\Gamma(p-v+1)p!} - \frac{(x/2)^{2p+v}}{\Gamma(p+v+1)p!} \right], \quad (38)$$

$$v \notin Z, |x| < \infty$$

and an alternative expression of the Q -function [37]

$$Q(x) = \frac{1}{\pi} \int_0^{\pi/2} \exp\left(-\frac{x^2}{2 \sin^2 \theta}\right) d\theta. \quad (39)$$

Substituting (1), (38), and (39) into (37), and after some algebra (see Appendix C), we can obtain an analytical lower bound in series form as

$$P_{e,PL}^{lower} = \frac{\Lambda(\alpha, \beta)}{2} \sum_{p=0}^{\infty} \left\{ a_p(\alpha, \beta) \left(\frac{\bar{\gamma}_{PL}^{MRC}}{2} \right)^{-(p+\beta)} B\left(\frac{1}{2}, p + \beta + \frac{1}{2}\right) \right. \\ \left. - a_p(\beta, \alpha) \left(\frac{\bar{\gamma}_{PL}^{MRC}}{2} \right)^{-(p+\alpha)} B\left(\frac{1}{2}, p + \alpha + \frac{1}{2}\right) \right\}, \quad (40)$$

where $B(x, y) = \int_0^1 t^{x-1} (1-t)^{y-1} dt$ is the Beta function, and

$$\Lambda(\alpha, \beta) = \frac{1}{\Gamma(\alpha)\Gamma(\beta) \sin[(\alpha - \beta)\pi]}; \quad (41)$$

$$a_p(x, y) = \frac{(xy)^{p+y} \Gamma(p+y)}{\Gamma(p-x+y+1)p!}.$$

In addition, by replacing $\bar{\gamma}_{PL}^{MRC}$ in (40) with $\bar{\gamma}_{SMF}$ and $\bar{\gamma}_{MMF}$, we can obtain the unconditional BER for SMF receiver and MMF receiver, respectively.

C. Truncation Error Analysis

To implement the series form lower bound BER in (40), we have to truncate the summation of infinite terms into a summation of finite terms. Therefore, it is necessary to analyze the truncation error. For simplicity, in the following we use $\bar{\gamma}$ to represent $\bar{\gamma}_{PL}^{MRC}$, $\bar{\gamma}_{SMF}$, and $\bar{\gamma}_{MMF}$. Substituting $B(x, y) = \frac{\Gamma(x)\Gamma(y)}{\Gamma(x+y)}$ [38, 8.384(1)] and $\Gamma(x+1) = x\Gamma(x)$ [38, 8.331(1)] into (40), we obtain the error probability as

$$P_e = \frac{\sqrt{\pi}}{2} \Lambda(\alpha, \beta) \sum_{p=0}^{\infty} \frac{1}{p!} \left(\frac{2\alpha\beta}{\bar{\gamma}} \right)^p \{G_p(\alpha, \beta) - G_p(\beta, \alpha)\}, \quad (42)$$

where $G_p(x, y)$ is defined as

$$G_p(x, y) = \frac{\Gamma(p + y + \frac{1}{2})}{(p + y)\Gamma(p - x + y + 1)} \left(\frac{2xy}{\bar{\gamma}}\right)^y. \quad (43)$$

Now we can estimate the truncation error caused by eliminating the infinite terms after the first J terms in (42). This truncation error can be defined as

$$\epsilon_J = \frac{\sqrt{\pi}}{2} \Lambda(\alpha, \beta) \sum_{p=J}^{\infty} \frac{1}{p!} \left(\frac{2\alpha\beta}{\bar{\gamma}}\right)^p \{G_p(\alpha, \beta) - G_p(\beta, \alpha)\}. \quad (44)$$

When $p \rightarrow \infty$, we have $G_p(\alpha, \beta) \rightarrow 0$ and $G_p(\beta, \alpha) \rightarrow 0$. Then we can obtain an upper bound of the truncation error as

$$\begin{aligned} \epsilon_J &< \frac{\sqrt{\pi}}{2} \Lambda(\alpha, \beta) \sum_{p=J}^{\infty} \frac{1}{p!} \left(\frac{2\alpha\beta}{\bar{\gamma}}\right)^p \max_{p \geq L} \{G_p(\alpha, \beta) - G_p(\beta, \alpha)\} \\ &< \frac{\sqrt{\pi}}{2} \frac{\Lambda(\alpha, \beta)}{J!} \left(\frac{2\alpha\beta}{\bar{\gamma}}\right)^J \exp\left(\frac{2\alpha\beta}{\bar{\gamma}}\right) \\ &\quad \times \max_{p \geq L} \{G_p(\alpha, \beta) - G_p(\beta, \alpha)\}, \end{aligned} \quad (45)$$

where in the last inequality we have used the Lagrange form for the remainder term of Taylor series expansion for the exponential function. Note that when J approaches ∞ , the term $\frac{1}{J!} \left(\frac{2\alpha\beta}{\bar{\gamma}}\right)^J$ approaches zero. Therefore, truncation error ϵ_J diminishes to zero with increasing index J . Besides, we can also observe that ϵ_J diminishes rapidly with the average SNR $\bar{\gamma}$. This suggests that the series lower bound solution is highly accurate in the large SNR regimes. We can therefore perform an asymptotic BER analysis.

D. Asymptotic Lower Bound For BER

We now examine the lower bound BER behavior in the large SNR regimes. When $\bar{\gamma} \rightarrow \infty$, we have $G_p(\alpha, \beta) \rightarrow 0$ and $G_p(\beta, \alpha) \rightarrow 0$. From (42) we know that the first term ($p = 0$) of the series summation becomes the dominant term in the large SNR regimes. Therefore, the unconditional lower bound BER in high SNR regimes can be approximated by

$$P_e \approx \frac{\sqrt{\pi}}{2} \Lambda(\alpha, \beta) [G_0(\alpha, \beta) - G_0(\beta, \alpha)]. \quad (46)$$

For typical turbulence conditions, we have $\alpha > \beta$. Then in high SNR regimes, we have

$$\frac{G_0(\beta, \alpha)}{G_0(\alpha, \beta)} = \frac{\beta\Gamma(\alpha + \frac{1}{2})\Gamma(-\alpha + \beta + 1)}{\alpha\Gamma(\beta + \frac{1}{2})\Gamma(-\beta + \alpha + 1)} \left(\frac{2\alpha\beta}{\bar{\gamma}}\right)^{\alpha-\beta} \ll 1. \quad (47)$$

Therefore, we can omit the second term in (46) and obtain

$$P_e \approx H(\alpha, \beta) \left(\frac{1}{\bar{\gamma}} \right)^\beta, \quad (48)$$

where

$$H(\alpha, \beta) = \frac{\sqrt{\pi}}{2} \frac{(2\alpha\beta)^\beta \Gamma(\beta + \frac{1}{2})}{\Gamma(\alpha)\Gamma(\beta + 1)\Gamma(-\alpha + \beta + 1) \sin[(\alpha - \beta)\pi]}. \quad (49)$$

This indicates that the asymptotic lower bound BERs in high SNR regimes of the coherent optical communication system based on PL receiver, SMF receiver, and MMF receiver are decayed exponentially by the average SNR with an exponential decay constant β .

V. NUMERICAL RESULTS

When the PL power distribution satisfies a general truncated multivariate Gaussian distribution and N is large, we have to count on the stochastic numerical integration methods to calculate the normalization constant C_2 , the average SNR and unconditional BER. However, the generation of random numbers satisfying truncated multivariate Gaussian distribution is not trivial. Here we use the Monte-Carlo integration (MCI) method (see Appendix D) to calculate them. We set the number of SMF ends as $N = 10$ in the following simulations. The turbulence parameters are $(\alpha = 2.23, \beta = 1.54)$ for moderate turbulence condition and $(\alpha = 2.34, \beta = 1.02)$ for strong turbulence condition [31]. For the PL based receiver, we consider three different Gaussian variances $\sigma^2 = 0$, $\sigma^2 = 0.01$, and $\sigma^2 = \infty$, which corresponds to the multivariate degenerate distribution, general truncated multivariate Gaussian distribution, and multivariate uniform distribution, respectively.

We first present the BERs of SMF receiver, MMF receiver, and PL based receiver using different combining techniques under moderate turbulence, shown in Fig. 5. We take the SMF receiver as the reference and the horizontal axis is the average SNR of the SMF receiver, i.e., $\bar{\gamma}_0 = \bar{\gamma}_{SMF}$. As we have demonstrated in Sections III and IV, the BER for MRC is irrelevant with the power distribution of the PL and it equals to the BER for EGC with degenerate distribution. From Fig. 5, we can see that the BER performance for EGC is much better than that for SC. Besides, the BERs for EGC under different PL power distributions are close to each other. The ratio of BER of $\sigma^2 = \infty$ over BER when $\sigma^2 = 0$ is around 1.3. This indicates that the PL power distribution has limited influence on the BER performance of the PL based receiver when EGC is used. However, the BER for SC of the uniform distribution ($\sigma^2 = \infty$) is much lower than that of the degenerate distribution ($\sigma^2 = 0$). The ratio of BER when $\sigma^2 = 0$ over BER when

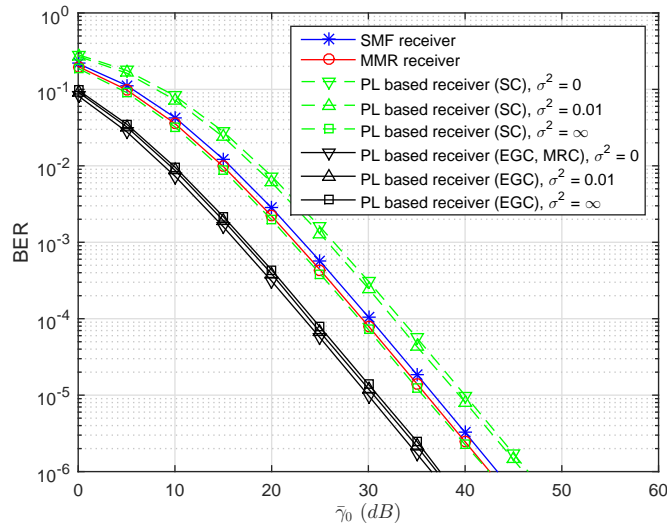


Fig. 5. The BER comparison between PL based receiver, SMF receiver, and MMF receiver for coherent FSOC system ($\xi_{PL} = 0.8$, $\frac{\eta_S}{\eta_M} = 5$, $\frac{\zeta_M}{\zeta_S} = 6$)

$\sigma^2 = \infty$ is around 4.8. This indicates that the PL power distribution can greatly affect the BER performance of the PL based receiver when SC is used.

Because the BERs for EGC under different PL power distributions are close to the BER for MRC and they are much better than the BER for SC under different PL power distributions, next we will focus on the performance comparison between the PL based receiver with EGC, the SMF receiver, and the MMF receiver.

The BER comparison between the PL based receiver with EGC, the SMF receiver, and the MMF receiver for coherent FSOC systems under the moderate and strong turbulence conditions is shown in Fig. 6. From Fig. 6, we can find that, when the BER is 10^{-6} , the $\bar{\gamma}_0$ for the PL based receiver with EGC, the MMF receiver, and the SMF under moderate turbulence are about 37 dB, 42.5 dB and 43 dB, respectively; and under strong turbulence are about 53 dB, 57.5 dB and 58 dB, respectively. This suggests that SMF receiver and MMF receiver require an additional 6 dB and 5.5 dB SNR to achieve the same BER as the PL based receiver with EGC under moderate turbulence; and require an additional 5 dB and 4.5 dB SNR to achieve the same BER as the PL based receiver with EGC under strong turbulence.

Then we present the average SNR gains of the PL based receiver with EGC over the SMF

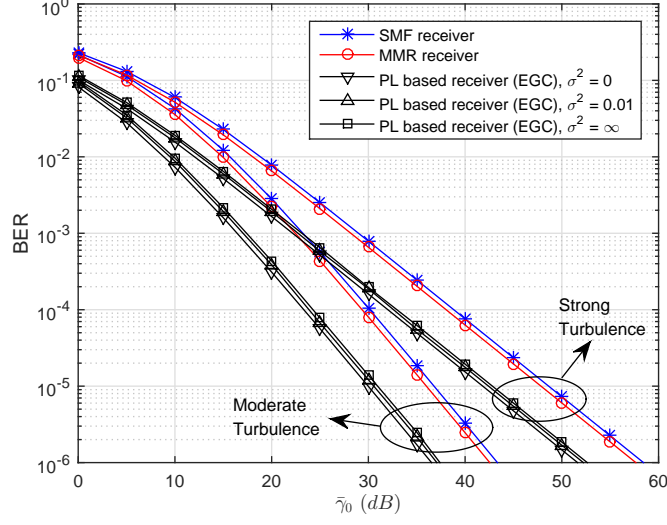


Fig. 6. The BER comparison between PL based receiver, SMF receiver, and MMF receiver for coherent FSOC system ($\xi_{PL} = 0.8$, $\frac{\eta_S}{\eta_M} = 5$, $\frac{\zeta_M}{\zeta_S} = 6$)

receiver $\bar{\gamma}_{PL}/\bar{\gamma}_{SMF} = \frac{\xi_{PL}}{N} \frac{\zeta_M}{\zeta_S} E \left[\left(\sum_{i=1}^N \sqrt{a_i} \right)^2 \right]$, and over the MMF receiver $\bar{\gamma}_{PL}/\bar{\gamma}_{MMF} = \frac{\xi_{PL}}{N} \frac{\eta_S}{\eta_M} E \left[\left(\sum_{i=1}^N \sqrt{a_i} \right)^2 \right]$ under various imperfect device parameters, including the coupling efficiency, the mixing efficiency, and the PL loss. We analyze the value of the coupling efficiencies of MMF, few-mode fiber and SMF in the literature [4], [6]–[11], [19], [20], and set the coupling efficiency gain of MMF over SMF as $\frac{\zeta_M}{\zeta_S} \in [0, 20]$. We analyze the value of the mixing efficiency of SMF and MMF in the literature [12]–[16], [39], and set the mixing efficiency gain of SMF over MMF as $\frac{\eta_S}{\eta_M} \in [4, 8]$. The range of the PL loss is set as $\xi_{PL} \in [0, 1]$.

Figures 7 and 8 show the obtained average SNR gain $\bar{\gamma}_{PL}^{EGC}/\bar{\gamma}_{SMF}$ and $\bar{\gamma}_{PL}^{EGC}/\bar{\gamma}_{MMF}$, respectively. The scope of application of the PL based receiver for FSOC systems can be obtained from Figs. 7 and 8: when $\bar{\gamma}_{PL}^{EGC}/\bar{\gamma}_{SMF} > 1$, we can choose to use the PL based receiver instead of SMF receiver for coherent FSOC systems; when $\bar{\gamma}_{PL}^{EGC}/\bar{\gamma}_{MMF} > 1$, we can choose to use the PL based receiver instead of MMF receiver for coherent FSOC systems. Besides, from Figs. 7 and 8, we can observe that the difference of the average SNR gain among three PL power distributions increases as average SNR gain increases. This indicates that the influence of the PL power distribution on the average SNR gain becomes significant in high SNR gain.

At last, we present the integral solution, series lower bound solution and the asymptotic

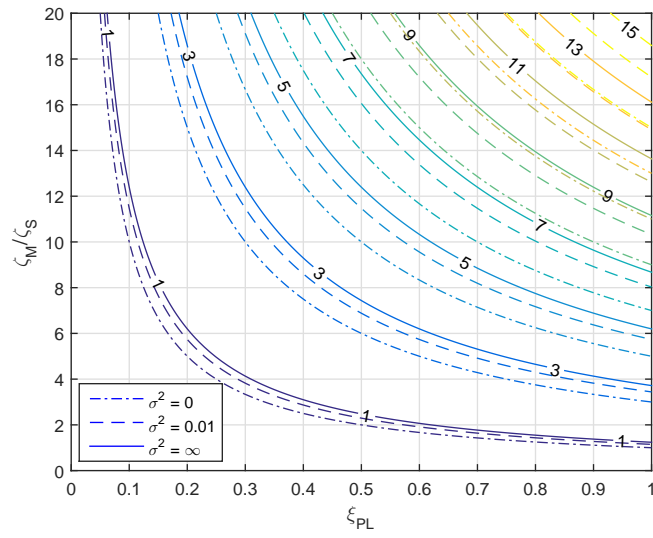


Fig. 7. The average SNR gain of PL based receiver over SMF receiver for coherent FSOC system

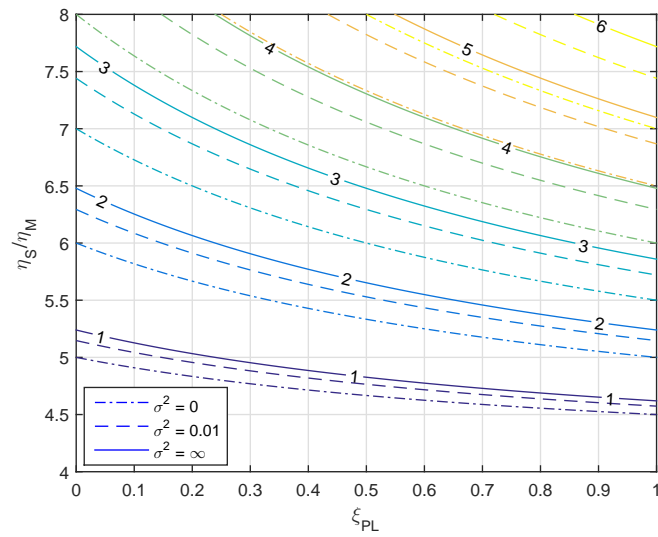


Fig. 8. The average SNR gain of PL based receiver over MMF receiver for coherent FSOC system

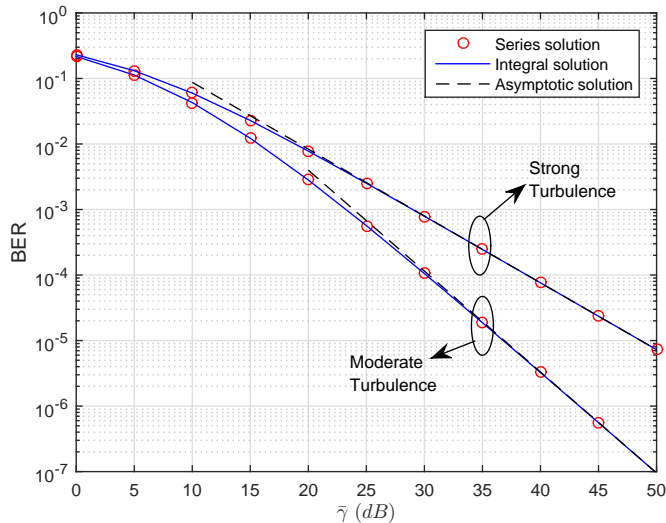


Fig. 9. Comparison between integral solution, series solution, and asymptotic solution of coherent FSOC system using PL based receiver.

solution of the unconditional lower bound BER in Fig. 9. The series lower bound solution is calculated by (40) with $J = 30$. We can see that the series lower bound solution is consistent with the integral solution, and the asymptotic lower bound BER approaches the exact BER curve in high SNR regimes ($\bar{\gamma} > 30$ dB).

VI. CONCLUSION

This paper proposed a truncated multivariate Gaussian distribution over a simplex for the power distribution at SMF ends of the PL. The SNR and BER for PL based receiver are analyzed using different combining techniques, including SC, EGC, and MRC; and they are compared with the SMF and MMF receivers for FSOC systems. We demonstrated that the power distribution of the PL has no effect on the SNR and BER performance of PL based receiver when MRC is used. Simulation results showed that the power distribution of the PL has limited influence on the BER performance of PL based receiver when EGC is used; and it can greatly affect the BER performance of the PL based receiver when SC is used. Besides, we quantified the SNR gains of the PL based receiver using EGC over the SMF and MMF receivers under different imperfect devices parameters; and provided the scope of application of the considered communication

system. These findings can provide some useful guidelines for the design of PL based receiver for FSOC systems.

We have to remark that the PL with N SMF ends requires N balanced photodetectors to detect the received beams. Therefore, the cost and the complexity of the PL based receiver are higher than those of the SMF receiver. To reduce the number of balanced photodetectors and lower the complexity of the receiver, in the future work we will combine hybrid combining techniques, e.g., the hybrid-selection/equal-gain combining [40], with PL based receiver.

ACKNOWLEDGEMENT

Bo Zhang acknowledges the support from the UCAS Joint PhD Training Program that allows her to conduct this research while she was visiting The University of British Columbia, Canada.

REFERENCES

- [1] F. Liu, J. Sun, X. Ma, P. Hou, G. Cai, Z. Sun, Z. Lu, and L. Liu, "New coherent laser communication detection scheme based on channel-switching method," *Appl. Opt.*, vol. 54, no. 10, pp. 2738–2746, Apr. 2015.
- [2] M. Shemis, A. Ragheb, E. Alkhazraji, M. Esmail, H. Fathallah, S. Alshebeili, and M. Khan, "Self-seeded quantum-dash laser based 5 m–128 gb/s indoor free-space optical communication," *Chin. Opt. Lett.*, vol. 15, no. 10, p. 100604, Oct. 2017.
- [3] D. Zhou, T. Cao, Y. Yang, J. Zhang, P. Wang, and B. Yang, "Symbol error rate performance analysis of soft-decision decoded mppm free space optical system over exponentiated weibull fading channels," *Chin. Opt. Lett.*, vol. 15, no. 5, p. 050602, May 2017.
- [4] Y. Dikmelik and F. M. Davidson, "Fiber-coupling efficiency for free-space optical communication through atmospheric turbulence," *Appl. Opt.*, vol. 44, no. 23, pp. 4946–4952, Aug. 2005.
- [5] R. Zhang, J. Wang, G. Zhao, and J. Lv, "Fiber-based free-space optical coherent receiver with vibration compensation mechanism," *Opt. Express*, vol. 21, no. 15, pp. 18 434–18 441, July 2013.
- [6] P. J. Winzer and W. R. Leeb, "Fiber coupling efficiency for random light and its applications to lidar," *Opt. Lett.*, vol. 23, no. 13, pp. 986–988, July 1998.
- [7] M. Toyoshima, "Maximum fiber coupling efficiency and optimum beam size in the presence of random angular jitter for free-space laser systems and their applications," *J. Opt. Soc. Am.*, vol. 23, no. 9, pp. 2246–2250, Sept. 2006.
- [8] M. E. Grein, O. Shatrovov, D. V. Murphy, B. S. Robinson, and D. M. Boroson, "A multimode fiber-coupled photon-counting optical receiver for the lunar laser communication demonstration," in *2014 Conference on Lasers and Electro-Optics (CLEO)-Laser Science to Photonic Applications*. IEEE, 2014, pp. 1–2.
- [9] J. Poliak, D. Giggenbach, R. M. Calvo, and D. Bok, "Fiber coupling and field mixing of coherent free-space optical beams in satellite communications," in *Free-Space Laser Communication and Atmospheric Propagation XXVIII*, vol. 9739. International Society for Optics and Photonics, Mar. 2016, p. 973913.
- [10] S. Arisa, Y. Takayama, H. Endo, R. Shimizu, M. Fujiwara, and M. Sasaki, "Coupling efficiency of laser beam to multimode fiber for free space optical communication," in *International Conference on Space Optics—ICSO 2014*, vol. 10563. International Society for Optics and Photonics, Nov. 2017, p. 105630Y.

- [11] B. Hu, L. Yu, and Y. Zhang, "Fiber coupling efficiency of gaussian-schell model beams in an ocean to fiber link with a zernike tilt correction," *Appl. Opt.*, vol. 57, no. 20, pp. 5831–5836, July 2018.
- [12] M. B. Mark, "A comparison of free space and fiber mixer performances in a heterodyne laser radar," in *Proceedings of the IEEE 1992 National Aerospace and Electronics Conference@ m_NAECON 1992*. IEEE, 1992, pp. 1256–1262.
- [13] B. D. Duncan, M. B. Mark, and P. F. McManamon, "Performance analysis of a heterodyne lidar system incorporating a multimode optical waveguide receiver," in *Proceedings of the IEEE 1993 National Aerospace and Electronics Conference-NAECON 1993*. IEEE, 1993, pp. 1133–1141.
- [14] D. K. Jacob, M. B. Mark, and B. D. Duncan, "Heterodyne lidar system efficiency enhancement using single-mode optical fiber mixers," *Opt. Eng.*, vol. 34, no. 11, pp. 3122–3130, Nov. 1995.
- [15] W. R. Leeb, P. J. Winzer, and K. H. Kudielka, "Aperture dependence of the mixing efficiency, the signal-to-noise ratio, and the speckle number in coherent lidar receivers," *Appl. Opt.*, vol. 37, no. 15, pp. 3143–3148, May 1998.
- [16] Y. Ren, A. Dang, L. Liu, and H. Guo, "Heterodyne efficiency of a coherent free-space optical communication model through atmospheric turbulence," *Appl. Opt.*, vol. 51, no. 30, pp. 7246–7254, Oct. 2012.
- [17] J. Niu and J. Xu, "Coupling efficiency of laser beam to multimode fiber," *Opt. Commun.*, vol. 274, no. 2, pp. 315–319, June 2007.
- [18] Y. Takayama, Y. Koyama, and M. Toyoshima, "Studies for simplified optical ground stations by using multimode fibers," *Technical report of IEICE. SAT*, vol. 111, no. 336, pp. 147–151, 2011.
- [19] D. Zheng, Y. Li, E. Chen, B. Li, D. Kong, W. Li, and J. Wu, "Free-space to few-mode-fiber coupling under atmospheric turbulence," *Opt. Express*, vol. 24, no. 16, pp. 18739–18744, Aug. 2016.
- [20] I. Ozdur, P. Toliver, and T. K. Woodward, "Photonic-lantern-based coherent lidar system," *Opt. Express*, vol. 23, no. 4, pp. 5312–5316, Feb. 2015.
- [21] I. Ozdur, P. Toliver, A. Agarwal, and T. Woodward, "Free-space to single-mode collection efficiency enhancement using photonic lanterns," *Opt. Lett.*, vol. 38, no. 18, pp. 3554–3557, Sept. 2013.
- [22] I. Ozdur, P. Toliver, and T. Woodward, "Performance improvements of photonic lantern based coherent receivers," in *2014 IEEE Photonics Conference*. IEEE, 2014, pp. 368–369.
- [23] R. Ryf, N. Fontaine, M. Montoliu, S. Randel, B. Ercan, H. Chen, S. Chandrasekhar, A. Gnauck, S. Leon-Saval, J. Bland-Hawthorn *et al.*, "Photonic-lantern-based mode multiplexers for few-mode-fiber transmission," in *Optical fiber communication conference*. Optical Society of America, Mar. 2014, pp. W4J–2.
- [24] B. Zhang, R. Yuan, J. Cheng, J. Sun, and S. Leon-Saval, "A study of power distributions in photonic lantern for coherent optical receiver," *IEEE Photon. Technol. Lett.*, vol. 31, no. 17, pp. 1465–1468, Sept. 2019.
- [25] S. G. Leon-Saval, T. Birks, J. Bland-Hawthorn, and M. Englund, "Multimode fiber devices with single-mode performance," *Opt. Lett.*, vol. 30, no. 19, pp. 2545–2547, Oct. 2005.
- [26] T. A. Birks, I. Gris-Sánchez, S. Yerolatsitis, S. Leon-Saval, and R. R. Thomson, "The photonic lantern," *Advances in Optics and Photonics*, vol. 7, no. 2, pp. 107–167, June 2015.
- [27] B. Huang, N. K. Fontaine, R. Ryf, B. Guan, S. G. Leon-Saval, R. Shubochkin, Y. Sun, R. Lingle, and G. Li, "All-fiber mode-group-selective photonic lantern using graded-index multimode fibers," *Opt. Express*, vol. 23, no. 1, pp. 224–234, Jan. 2015.
- [28] S. G. Leon-Saval, N. K. Fontaine, J. R. Salazar-Gil, B. Ercan, R. Ryf, and J. Bland-Hawthorn, "Mode-selective photonic lanterns for space-division multiplexing," *Opt. Express*, vol. 22, no. 1, pp. 1036–1044, Jan. 2014.
- [29] Y. Li, Y. Li, L. Feng, C. Yang, W. Li, J. Qiu, X. Hong, Y. Zuo, H. Guo, W. Tong *et al.*, "Mode-selective photonic lanterns for orbital angular momentum mode division multiplexing," *Applied Sciences*, vol. 9, no. 11, p. 2233, June 2019.

- [30] D. Zheng, Y. Li, H. Zhou, Y. Bian, C. Yang, W. Li, J. Qiu, H. Guo, X. Hong, Y. Zuo *et al.*, "Performance enhancement of free-space optical communications under atmospheric turbulence using modes diversity coherent receipt," *Opt. Express*, vol. 26, no. 22, pp. 28 879–28 890, Oct. 2018.
- [31] A. Al-Habash, L. C. Andrews, and R. L. Phillips, "Mathematical model for the irradiance probability density function of a laser beam propagating through turbulent media," *Opt. Eng.*, vol. 40, no. 8, pp. 1554–1563, Aug. 2001.
- [32] N. D. Chatzidiamantis and G. K. Karagiannidis, "On the distribution of the sum of gamma-gamma variates and applications in rf and optical wireless communications," *IEEE Trans. Commun.*, vol. 59, no. 5, pp. 1298–1308, May 2011.
- [33] K. Li, J. Ma, L. Tan, S. Yu, and C. Zhai, "Performance analysis of fiber-based free-space optical communications with coherent detection spatial diversity," *Appl. Opt.*, vol. 55, no. 17, pp. 4649–4656, June 2016.
- [34] S. Onn and I. Weissman, "Generating uniform random vectors over a simplex with implications to the volume of a certain polytope and to multivariate extremes," *Ann. Oper. Res.*, vol. 189, no. 1, pp. 331–342, Sept. 2011.
- [35] S. Wilhelm and B. Manjunath, "tmvtnorm: A package for the truncated multivariate normal distribution," *Sigma*, vol. 2, no. 2, June 2010.
- [36] X. Song, M. Niu, and J. Cheng, "Error rate of subcarrier intensity modulations for wireless optical communications," *IEEE Commun. Lett.*, vol. 16, no. 4, pp. 540–543, Apr. 2012.
- [37] J. Park, E. Lee, and G. Yoon, "Average bit-error rate of the alamouti scheme in gamma-gamma fading channels," *IEEE Photon. Technol. Lett.*, vol. 23, no. 4, pp. 269–271, Feb. 2010.
- [38] I. S. Gradshteyn and I. M. Ryzhik, *Table of Integrals, Series, and Products*. Academic press, 2014.
- [39] R. G. Marshalek, G. S. Mecherle, and P. Jordan, "System-level comparison of optical and rf technologies for space-to-space and space-to-ground communication links circa 2000," in *Free-Space Laser Communication Technologies VIII*, vol. 2699. International Society for Optics and Photonics, Conference Proceedings, pp. 134–146.
- [40] Y. Ma and J. Jin, "Unified performance analysis of hybrid-selection/equal-gain combining," *IEEE Trans. Veh. Technol.*, vol. 56, no. 4, pp. 1866–1873, July 2007.
- [41] R. Yuan, J. Ma, P. Su, Y. Dong, and J. Cheng, "Monte-carlo integration models for multiple scattering based optical wireless communication," *IEEE Trans. Commun.*, vol. 68, no. 1, pp. 334–348, Jan. 2019.

APPENDIX A

DERIVATION OF $f(\mathbf{a})$

Substituting (7) into (5) and letting $\rho \rightarrow -\frac{1}{N-1}$, we can obtain

$$\begin{aligned}
f(\mathbf{a}) &= \lim_{\rho \rightarrow -\frac{1}{N-1}} \frac{1}{C_1} \exp \left\{ -\frac{1}{2} \frac{[1 + (N-2)\rho] \sum_{i=1}^N x_i^2 - 2\rho \sum_{i=1}^{N-1} \sum_{j=i+1}^N x_i x_j}{[1 + (N-1)\rho](1-\rho)\sigma^2} \right\} \\
&= \lim_{\rho \rightarrow -\frac{1}{N-1}} \frac{1}{C_1} \exp \left\{ -\frac{1}{2} \frac{[1 + (N-3)\rho] \sum_{i=1}^{N-1} x_i^2 - 2\rho \sum_{i=1}^{N-1} \sum_{j=i+1}^{N-2} x_i x_j}{(1-\rho)[1 + (N-2)\rho]\sigma^2} \right\} \\
&\quad \underbrace{\hspace{15em}}_{H_1} \\
&\quad \times \lim_{\rho \rightarrow -\frac{1}{N-1}} \exp \left\{ -\frac{1}{2} \frac{\left[x_N - \frac{\rho}{1+(N-2)\rho} \sum_{i=1}^{N-1} x_i \right]^2}{\varepsilon^2} \right\}, \\
&\quad \underbrace{\hspace{15em}}_{H_2}
\end{aligned} \tag{50}$$

where $x_i = a_i - \frac{1}{N}$ and $\varepsilon = \sigma \sqrt{\frac{[1+(N-1)\rho](1-\rho)}{[1+(N-2)\rho]}}$.

When $\rho \rightarrow -\frac{1}{N-1}$, we have $\varepsilon \rightarrow 0$. Because the limit of the Gaussian distribution can be expressed as the Dirac delta function, then we can simplify H_2 in (50) as

$$\begin{aligned}
H_2 &= \lim_{\rho \rightarrow -\frac{1}{N-1}} \sqrt{2\pi\varepsilon^2} \times \delta \left[x_N - \frac{\rho}{1+(N-2)\rho} \sum_{i=1}^{N-1} x_i \right] \\
&= \lim_{\rho \rightarrow -\frac{1}{N-1}} \sqrt{2\pi\varepsilon^2} \times \delta(a_1 + a_2 + \cdots + a_N - 1),
\end{aligned} \tag{51}$$

where $\delta(\cdot)$ is the Dirac delta function. Using the expression in (7), we can simplify H_1 in (50) as

$$H_1 = \frac{1}{C_1} \exp \left\{ -\frac{1}{2} [\mathbf{a}^* - \boldsymbol{\mu}_{\mathbf{a}^*}]^T \boldsymbol{\Sigma}_{\mathbf{a}^*}^{-1} [\mathbf{a}^* - \boldsymbol{\mu}_{\mathbf{a}^*}] \right\}. \tag{52}$$

Substituting (51) and (52) into (50), we can obtain

$$\begin{aligned}
f(\mathbf{a}) &= \lim_{\rho \rightarrow -\frac{1}{N-1}} \frac{\sqrt{2\pi\varepsilon^2}}{C_1} \exp \left\{ -\frac{1}{2} [\mathbf{a}^* - \boldsymbol{\mu}_{\mathbf{a}^*}]^T \boldsymbol{\Sigma}_{\mathbf{a}^*}^{-1} [\mathbf{a}^* - \boldsymbol{\mu}_{\mathbf{a}^*}] \right\} \\
&\quad \times \delta(a_1 + a_2 + \cdots + a_N - 1).
\end{aligned} \tag{53}$$

We can find that there exists the same factor $\sqrt{2\pi\varepsilon^2}$ in the numerator and denominator C_1 . Finally, by eliminating the term $\sqrt{2\pi\varepsilon^2}$ in both numerator and denominator, the joint PDF in (9) can be obtained.

APPENDIX B

DERIVATION OF $E[\sqrt{a_1 a_2}]$ FOR UNIFORM DISTRIBUTION

The mathematical expectation of $\sqrt{a_1 a_2}$ for a joint PDF $f(\mathbf{a})$ in (15) is defined as

$$\begin{aligned} E[\sqrt{a_1 a_2}] &= (N-1)! \int_0^1 \sqrt{a_1} \int_0^{1-a_1} \sqrt{a_2} \int_0^{1-a_1-a_2} \cdots \int_0^{1-a_1-\cdots-a_{N-1}} \\ &\quad \times \delta(a_1 + a_2 + \cdots + a_N - 1) da_1 da_2 \cdots da_N \\ &= (N-1)! \int_0^1 \sqrt{a_1} \int_0^{1-a_1} \sqrt{a_2} \int_0^{1-a_1-a_2} \cdots \int_0^{1-a_1-\cdots-a_{N-2}} da_1 da_2 \cdots da_{N-1}. \end{aligned} \quad (54)$$

By integrating a_{N-1} out, we can obtain

$$\begin{aligned} E[\sqrt{a_1 a_2}] &= (N-1)! \int_0^1 \sqrt{a_1} \int_0^{1-a_1} \sqrt{a_2} \int_0^{1-a_1-a_2} \cdots \int_0^{1-a_1-\cdots-a_{N-3}} \\ &\quad \times \frac{1}{1!} (1 - a_1 - a_2 - \cdots - a_{N-2}) da_1 da_2 \cdots da_{N-2}. \end{aligned} \quad (55)$$

By integrating a_{N-2} out, we can obtain

$$\begin{aligned} E[\sqrt{a_1 a_2}] &= (N-1)! \int_0^1 \sqrt{a_1} \int_0^{1-a_1} \sqrt{a_2} \int_0^{1-a_1-a_2} \cdots \int_0^{1-a_1-\cdots-a_{N-4}} \\ &\quad \times \frac{1}{2!} (1 - a_1 - a_2 - \cdots - a_{N-3})^2 da_1 da_2 \cdots da_{N-3}. \end{aligned} \quad (56)$$

Similarly, by successively integrating $a_{N-3}, a_{N-4}, \cdots, a_3$ out, we can obtain

$$\begin{aligned} E[\sqrt{a_1 a_2}] &= (N-1)! \int_0^1 \sqrt{a_1} \int_0^{1-a_1} \sqrt{a_2} \frac{1}{(N-3)!} (1 - a_1 - a_2)^{N-3} da_1 da_2 \\ &= (N-1)(N-2) \int_0^1 \sqrt{a_1} \int_0^{1-a_1} \sqrt{a_2} (1 - a_1 - a_2)^{N-3} da_1 da_2. \end{aligned} \quad (57)$$

Using the relation of Beta function $\int_a^b (t-a)^{x-1} (b-t)^{y-1} dt = (b-1)^{x+y-1} B(x, y)$ [38, 3.196(3)], we can obtain

$$E[\sqrt{a_1 a_2}] = (N-1)(N-2) B\left(\frac{3}{2}, N - \frac{1}{2}\right) B\left(\frac{3}{2}, N - 2\right). \quad (58)$$

Using the equalities $B(x, y) = \frac{\Gamma(x)\Gamma(y)}{\Gamma(x+y)}$ [38, 8.384(1)], $\Gamma(\frac{3}{2}) = \frac{\pi}{4}$, and $\Gamma(m) = (m-1)!$, we can obtain

$$E[\sqrt{a_1 a_2}] = \frac{\pi}{4N}. \quad (59)$$

APPENDIX C

DERIVATION OF THE ANALYTICAL EXPRESSION FOR $P_{e,PL}^{lower}$

Substituting (1), (38), and (39) into (37), we can obtain

$$P_{e,PL}^{lower} = \Lambda(\alpha, \beta) \int_0^{\pi/2} \int_0^\infty \left\{ \sum_{p=0}^\infty \left[\frac{a_p(\alpha, \beta) I^{p+\beta-1}}{\Gamma(p+\beta)} \exp\left(-\frac{\bar{\gamma}_{PL}^{MRC} I}{2 \sin^2 \theta}\right) \right] - \sum_{p=0}^\infty \left[\frac{a_p(\beta, \alpha) I^{p+\alpha-1}}{\Gamma(p+\alpha)} \exp\left(-\frac{\bar{\gamma}_{PL}^{MRC} I}{2 \sin^2 \theta}\right) \right] \right\} dI d\theta, \quad (60)$$

where $\Lambda(\alpha, \beta)$ and $a_p(x, y)$ are defined in (41).

Using $\int_0^\infty x^m \exp(-\beta x^n) dx = \frac{\Gamma(\frac{m+1}{n})}{n\beta^{\frac{m+1}{n}}}$ [38, 3.326(2)], we can obtain

$$P_{e,PL,Deg} = \Lambda(\alpha, \beta) \sum_{p=0}^\infty \int_0^{\pi/2} \left\{ a_p(\alpha, \beta) \left(\frac{\bar{\gamma}_{PL}^{MRC}}{2}\right)^{-(p+\beta)} \sin^{2p+2\beta} \theta - a_p(\beta, \alpha) \left(\frac{\bar{\gamma}_{PL}^{MRC}}{2}\right)^{-(p+\alpha)} \sin^{2p+2\alpha} \theta \right\} d\theta. \quad (61)$$

Using the Beta function $B(x, y) = 2 \int_0^{\pi/2} \sin^{2x-1} \psi \cos^{2y-1} \psi d\psi$ [38, 8.380(2)] and $B(x, y) = B(y, x)$ [38, 8.384(1)] into (61), we can obtain the series solution to the unconditional BER as (40).

APPENDIX D

MCI METHOD FOR CALCULATING C_2 , $\bar{\gamma}_{PL}$, $P_{out,PL}$, AND $P_{e,PL}$

In an MCI method, to obtain the integral result of $\int_{\mathbf{x}} g(\mathbf{x}) d\mathbf{x}$, we first choose a PDF $f(\mathbf{x})$, which is referred as the sampling function, and rewrite the integral as $\int_{\mathbf{x}} f(\mathbf{x}) \frac{g(\mathbf{x})}{f(\mathbf{x})} d\mathbf{x}$. Then the integral can be viewed as the mathematical expectation of the objective function $O(\mathbf{x}) \triangleq \frac{g(\mathbf{x})}{f(\mathbf{x})}$ when \mathbf{x} subjects to a PDF $f(\mathbf{x})$, i.e., $\int_{\mathbf{x}} f(\mathbf{x}) O(\mathbf{x}) d\mathbf{x} = E[\frac{g(\mathbf{x})}{f(\mathbf{x})}]$. Therefore, we can generate M samples $\{\mathbf{x}_1, \mathbf{x}_2, \dots, \mathbf{x}_M\}$ of \mathbf{x} according to the PDF $f(\mathbf{x})$ and use the average value of the objective function $\frac{1}{M} \sum_{m=1}^M O(\mathbf{x}_m)$ to estimate the mathematical expectation [41].

For example, to obtain the normalization constant C_2 , we can first rewrite C_2 as

$$C_2 = \int_{-\infty}^\infty \cdots \int_{-\infty}^\infty f_{MG}(\mathbf{a}) C_3 I_n(\mathbf{a}) da_1 \cdots da_N, \quad (62)$$

where $C_3 = [2\pi\sigma^2 N / (N-1)]^{\frac{N-1}{2}} / \sqrt{N}$ [24]; $f_{MG}(\mathbf{a})$ is the PDF of multivariate Gaussian variables $\mathbf{a} = [a_1, a_2, \dots, a_N]^T$ satisfying $a_1 + a_2 + \cdots + a_N = 1$, and $f_{MG}(\mathbf{a})$ is given by [24]

$$f_{MG}(\mathbf{a}) = \frac{1}{C_3} \exp\left\{-\frac{1}{2}[\mathbf{a}^* - \boldsymbol{\mu}_{\mathbf{a}^*}]^T \boldsymbol{\Sigma}_{\mathbf{a}^*}^{-1} [\mathbf{a}^* - \boldsymbol{\mu}_{\mathbf{a}^*}]\right\} \times \delta(a_1 + a_2 + \cdots + a_N - 1) \quad (63)$$

and $I_n(\mathbf{a})$ is an indicator function defined as

$$I_n(\mathbf{a}) = \begin{cases} 1, & \mathbf{a} \in V \\ 0, & \mathbf{a} \notin V. \end{cases} \quad (64)$$

Then we can choose $f_{MG}(\mathbf{a})$ as the sampling function and the objective function becomes $O(\mathbf{a}) = C_3 I_n(\mathbf{a})$. The generation of random numbers $\{a_1, a_2, \dots, a_N\}$ satisfying PDF $f_{MG}(\mathbf{a})$ can be achieved by two steps: first generate $\{a_1, a_2, \dots, a_{N-1}\}$ according to the $N - 1$ dimensional multivariate Gaussian PDF

$$f_{MG}(\mathbf{a}^*) = \frac{1}{C_3} \exp \left\{ -\frac{1}{2} [\mathbf{a}^* - \boldsymbol{\mu}_{\mathbf{a}^*}]^T \boldsymbol{\Sigma}_{\mathbf{a}^*}^{-1} [\mathbf{a}^* - \boldsymbol{\mu}_{\mathbf{a}^*}] \right\}; \quad (65)$$

then a_N is obtained as $a_N = 1 - a_1 - a_2 - \dots - a_{N-1}$.

The average SNR and the unconditional BER can be calculated in a similar method. In addition, to calculate the average SNR and the unconditional BER for uniform distribution case, the key is to generate the random numbers $\{a_1, a_2, \dots, a_N\}$ satisfying multivariate uniform distribution over the standard simplex. This can be achieved by the Algorithm 2 given in [34].